
ALLOY DESIGN IN THE SYSTEM FE-C-B

M.Sc. Jonathan Lentz, Dr.-Ing. Arne Röttger, Prof. Dr.-Ing. W. Theisen

Lehrstuhl Werkstofftechnik, Ruhr-Universität Bochum, 44801 Bochum, Germany

Lentz@wtech.rub.de, phone: +49(0)234-32-25967, fax: + 49(0)234-32-14104

ABSTRACT

In this study, the Fe-C-B system is used as a basis for alloy development of tool steels. Thereby, boron is used as hard phase forming element. The effect of chromium on the phase stability, microstructure and hard phase properties of Fe-C-B-Cr alloys is investigated. In this manner, thermodynamic equilibrium calculations are performed and experimentally validated. Laboratory alloys were casted and investigated using scanning electron microscopy (SEM), energy dispersive spectroscopy (EDS) and electron backscatter diffraction (EBSD). Nanoindentation was performed to investigate the effect of Cr on the micromechanical properties of the particular hard phases (elastic modulus and indentation hardness). It is shown, that Cr stabilizes the orthorhombic, Cr-rich M_2B type boride with a hardness of 22.8 GPa. In addition Cr stabilizes the Cr-rich $M_{23}(C,B)_6$ carboboride, which possess a lower hardness (14 GPa). In a next step, the findings are implemented in an alloy development and alloying additions of chromium, silicon and manganese are used to specifically stabilize the M_2B type boride with high Cr content to adjust a high hardness of the M_2B phase. Subsequently, a scratch test is performed to investigate the governing wear mechanisms in the developed alloy.

KEYWORDS

Steel development, tool steel, boron, hard phase properties, nanoindentation, CALPHAD

INTRODUCTION

A cost effective material, developed to withstand high wear attack, is tool steel. This group of steel is used for highly stressed parts for example in the field of mining or metal processing. Nevertheless, the durability of tool steels is still limited due to wear. Thereby, the major wear mechanism is grooving wear by hard counter bodies (abrasion). Consequently, the continuous development of tool steels with enhanced wear resistance is of high macroeconomic interest.

A metallurgical approach to maintain a high resistance against abrasion is realized through a sufficient amount of hard phases (5~15 vol.-%) which are embedded inside a tough metallic matrix. To optimize wear resistance, volume content, morphology and distribution of the hard phases should be individually adapted to the tribological system and to the interaction with the abrasive objects. Besides, an important parameter influencing the performance for wear protection applications are the hard phases' micromechanical properties. In this context, a comparison of different types of hard phases namely carbides, nitrides and borides shows that borides generally are favorable in terms of hardness. Hence, it seems likely to utilize Boron (B) as hard phase forming element in tool steels [1,2]. In this approach carbides, which are commonly used as hard phases and require high amounts of expensive or short resources such as vanadium or tungsten, are substituted by borides. These borides are formed with cheaper and widely available elements like iron (Fe), manganese (Mn) or chromium (Cr). The element carbon (C) is then primarily used to maintain the hardenability of the iron matrix and is uncoupled from formation of hard phases. Concluding, the utilization of B is promising to enhance application properties and at the same time to reduce the cost.

In this study, the systematic alloy design based on the Fe-C-B system is presented. Thermodynamic equilibrium calculations are used to design laboratory alloys. In this manner, the alloying elements Cr, Si and Mn are used to systematically adjust the phase content and the chemical composition of particular phases. Furthermore, the mechanical properties of the hard

phases are optimized with an adapted chemical composition of the hard phases. The calculations are experimentally validated using laboratory alloys. The microstructures of these alloys are investigated using scanning electron microscopy (SEM), energy dispersive X-ray spectroscopy (EDS) and electron backscatter diffraction (EBSD). Furthermore, the hardness and elastic modulus of the particular phases is measured using the nanoindentation technique. Finally, a scratch test is performed to investigate the governing micromechanical effects, concerning the wear-protection by the embedded hard phases.

1. EXPERIMENTAL PROCEDURE

Thermodynamic equilibrium calculations based on the CALPHAD method were used to design the phase content and chemical composition of the particular phases present in the alloy using the software ThermoCalc version S. Thermodynamic data were taken from the database TCFE6.2. The phases, LIQUID, FCC_A1, BCC_A2, CEMENTITE, M₂B_{tetr}, M₂₃C₆, and Cr₂B_{orth}, were regarded in the calculation. Furthermore, a pressure of 10³ mbar and an amount of quantity of 1 mol were taken into account.

Laboratory melts are manufactured to validate the equilibrium calculations and to investigate the microstructure and micromechanical properties of the alloys. In order to allow comparability of the thermodynamic equilibrium calculations and the laboratory melts, specimens were cut from the casting and heat-treated with regard to a hardening temperature of 900 or 1000 °C for 200 h in an inert gas furnace with argon atmosphere present and subsequently quenched in water.

Table 1: Chemical composition of the laboratory melts measured by optical emission spectrometry in mass% and hardening temperature T in °C

Alloy	T in °C	C	B	Cr	Si	Mn	Fe
0.6C-0.6B	1000	0.71	0.76	0.01	0.11	0.02	Bal.
0.6C-1.8B		0.69	1.92	0.03	0.16	0.02	Bal.
0.6C-0.6B-2.5Cr		0.58	0.66	2.25	0.11	0.01	Bal.
0.6C-0.6B-7.5Cr		0.59	0.57	6.75	0.14	0.02	Bal.
0.6C-0.6B-12.5Cr		0.59	0.57	11.86	0.16	0.02	Bal.
0Cr	900	0.75	1.98	0.04	2.27	3.81	Bal.
10Cr		0.65	1.97	10.00	2.41	3.77	Bal.

Prior to the microstructural examinations, the specimens were sectioned, ground on abrasive paper, and polished stepwise with 6 µm, 3 µm, and 1 µm diamond suspensions and etched with 3% alcoholic HNO₃. The microstructure of the specimens was investigated using the SEM Tescan MIRA3 in backscatter electron contrast (BSE) at a working distance of 7 mm and an acceleration voltage of 20 kV. The Cr content of the respective phases was measured using EDS system OXFORD X-Max 50 at a working distance of 15 mm and an electron-beam current of 5 nA. EBSD measurements were performed using the EBSD detector NordlysNano by Oxford instruments.

Hardness and elastic modulus of the respective phases were measured using the in-situ indentation module NanoFlip (Nanomechanics, inc.), using a diamond, cube corner indenter and a load of 50 mN at a constant strain rate of 0.2%/s and dynamic indentation method. Hardness and elastic modulus were evaluated as an average value for an indentation depth between 600-850 nm applying the method of Oliver and Pharr. For the estimation of elastic modulus, the Poisson ratio of the M₂B was assumed to be a constant value of 0.25, for M₃(C,B) and M₂₃(C,B)₆ phases a value of 0.36 was taken into account [3–6]. The indentation hardness was converted to Vickers hardness scale for reasons of comparability, knowing that the minimal indentation depth of 6 µm with regard to DIN EN ISO 14577 was not achieved [7]. Scratch testing was performed using the scratch module NST by CSM instruments, a conical diamond indenter with a tip radius of 2 µm and a constant load of 100 mN for a scratch length of 600 µm (speed 150 µm/min).

2. RESULTS & DISCUSSION

Fig. 1 a) is showing the quasi-binary phase diagram of the Fe-C-B system for a constant C content of 0.6 mass%, calculated with ThermoCalc, whereby the C content of 0.6 mass% is regarded to maintain the martensitic hardenability of the iron matrix. The Fe-0.6C-B system shows borides/carborborides of Fe_2B , $\text{Fe}_3(\text{C},\text{B})$ and $\text{Fe}_{23}(\text{C},\text{B})_6$ type, which are present besides the α -Fe and γ -Fe iron phases. The hypoeutectic region is located at B contents smaller than 3.4 mass% B and characterized by the primary solidification of γ -Fe cells. Higher B contents are stabilizing the primary solidification of the Fe_2B phase. The low melting phase of the system is $\text{Fe}_3(\text{C},\text{B})$. At temperatures between 800 and 600 °C the $\text{Fe}_3(\text{C},\text{B})$ phase becomes thermodynamically unstable and the $\text{Fe}_{23}(\text{C},\text{B})_6$ phase (τ -phase) is formed due to this miscibility gap. The B solubility of the $\text{Fe}_3(\text{C},\text{B})$ phase is decreasing with lower temperatures and thus the Fe_2B phase is stabilized through the release of B at temperatures smaller than 600 °C.

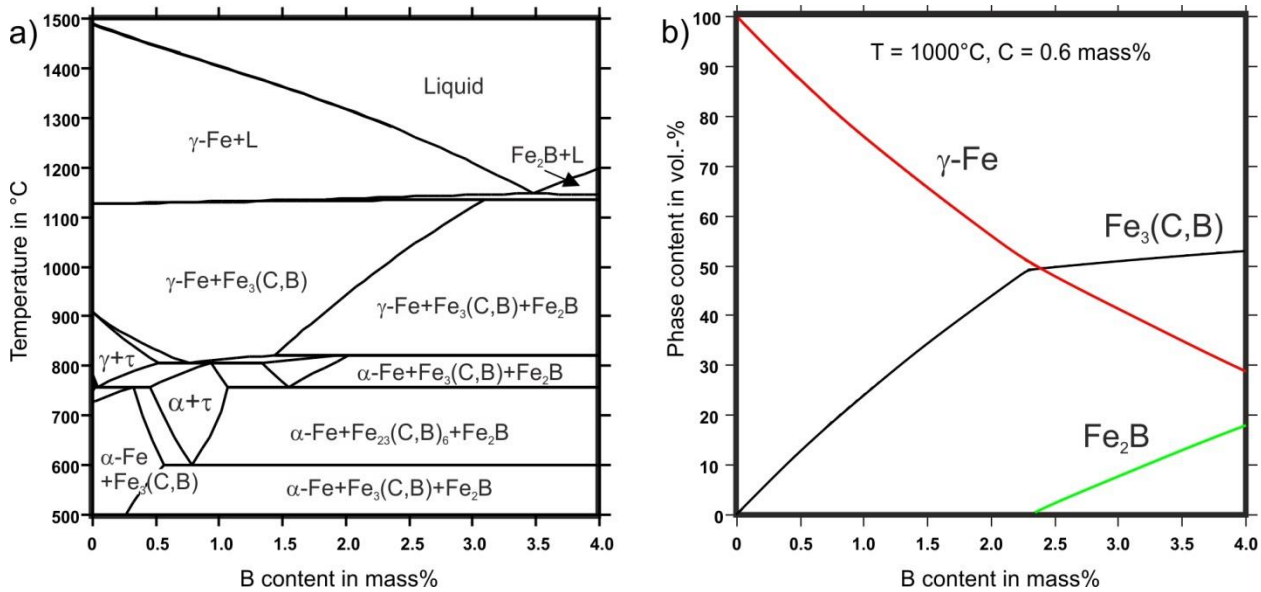


Fig. 1: a) Quasi-binary cross-section of the Fe-C-B system (constant C content of 0.6 mass%) b) Phase content in Fe-0.6C-B alloys at 1000 °C calculated with TC

The interdependence of the B content and the volume content of the particular phases that are present in Fe-0.6C-B alloy at a temperature of 1000 °C is depicted in Fig. 1 b). At low B contents, the volume content of the $\text{Fe}_3(\text{C},\text{B})$ phase is increasing almost linear with a slope of 22 vol.-% per mass% B until the Fe_2B phase is stabilized at a content of 2.3 mass% B. Furthermore, the volume content of the Fe_2B phase is increasing with 9 vol.-%, and the $\text{Fe}_3(\text{C},\text{B})$ phase with 2.5 vol.-% per mass% B. Following, B contents greater than 2.3 mass% are required to stabilize the Fe_2B phase in the Fe-C-B system, which is connected to a high volume content (> 50 vol.-%) of the $\text{Fe}_3(\text{C},\text{B})$ hard phase.

In Fig. 2 the microstructures of the 0.6C-0.6B (Fig. 2 a) and 0.6C-1.8B (Fig. 2b) are shown. A coarsened eutectic structure consisting of 14.8 vol.-% $\text{Fe}_3(\text{C},\text{B})$ phase in case of alloy 0.6C-0.6B and 40.5 vol.-% $\text{Fe}_2\text{B} + \text{Fe}_3(\text{C},\text{B})$ phases in case of alloy 0.6C-1.8B is present besides a martensitic iron matrix. In contrast to the thermodynamic calculations shown in Fig. 1, the Fe_2B phase is present at a B content below 2.3 mass%. This can be attributed to the technical non-equilibrium solidification process, whereby B is segregating in the remaining melt and the Fe_2B phase is stabilized [8].

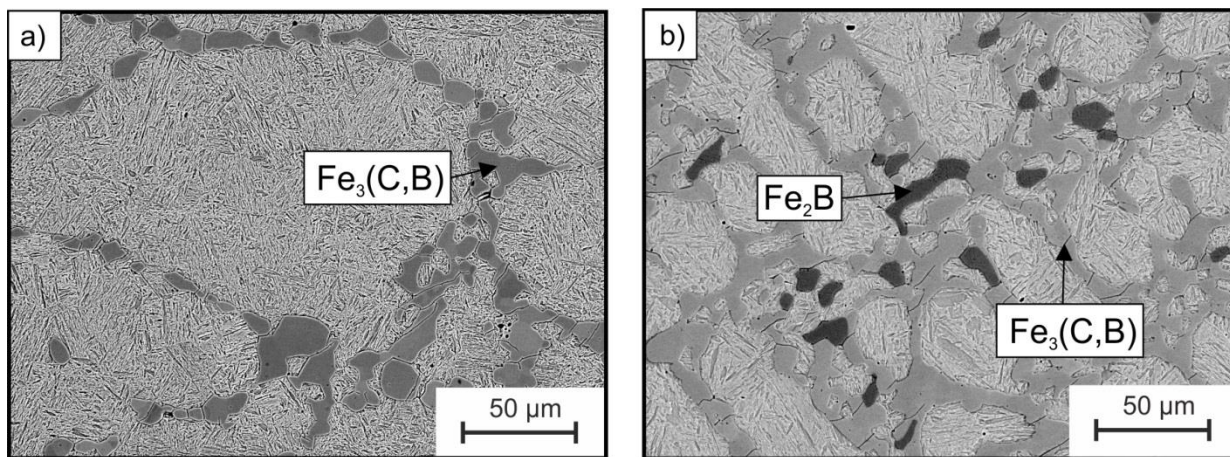


Fig. 2: SEM image of a) alloy 0.6C-0.6B and b) 0.6C-1.8B in BSE contrast

Against the background of alloy design, the most important parameters concerning the hard phases are mechanical properties like high hardness, elastic modulus and fracture toughness. In addition, a low C solubility of the hard phases is required following the alloying approach to use B as hard phase forming element and preserve C for matrix hardening. In this context, a low metal to metalloid ratio is beneficial to reduce the chemical-binding of expensive alloying elements. In addition, the Fe_2B phase has the highest hardness of the Fe-C-B system's hard phases (~1600 HV), shows only marginal C solubility and also a low metal to metalloid ratio ($M/(B+C)=2$) [9,10]. In contrast, the $\text{Fe}_{23}(\text{C,B})_6$ phase has a lower hardness (1100 HV), high metal to metalloid ratio ($M/(C+B)=3.83$) and a high solubility for C. The $\text{Fe}_3(\text{C,B})$ phase shows high solubility for both C and B, whereby the chemical composition and the micromechanical properties are dependent on the temperature region of formation. I.e. eutectic $\text{Fe}_3(\text{C,B})$ shows B contents up to 22 atom% and a hardness around 1300-1400 HV [11]. Concluding, the Fe_2B phase is beneficial in terms of micromechanical properties. Although, the Fe_2B phase is stabilized by the more pronounced B segregation occurring during technical solidification processes through, a stabilization of Fe_2B in the ternary Fe-C-B system requires high B contents, which is connected to hard phase contents greater than 45-50 vol.-%. Regarding the alloy development of steels, sufficient fracture toughness and forming capacity cannot be achieved with a volume content >15-20 vol.-%.

In this context, the element Cr can be used to further stabilize the orthorhombic M_2B type boride, which exceeds the mechanical properties of the hard phase M_7C_3 (~ 1400-1600 HV, $6.3\text{MPa}\sqrt{m}$) [12–14]. The effect of Cr addition on the phase stability and composition of the particular phases at a temperature of 1000 °C is shown in Fig. 3, whereby the B and C content of alloy 0.6C-0.6B is taken into account. Fig. 3 a) is showing the influence of the overall Cr content on the phase quantity of the particular phases (in vol.-%) that are present in alloy 0.6C-0.6B-xCr. At a Cr content of 0 mass%, 16 vol.-% $\text{M}_3(\text{C,B})$ phase is present. Furthermore, it becomes evident, that the $\text{M}_3(\text{C,B})$ phase is vanishing in favor of 10 vol.-% of $\text{M}_{23}(\text{C,B})_6$ and 5 vol.-% of M_2B phase at a Cr-content of ~1 mass%. Moreover, the M_2B phase is transforming from a tetragonal into an orthorhombic crystal structure above a Cr content of 4.5 mass%. At the same time, the volume content of the M_2B phase is slightly increasing from 5 vol.-% at 4.5 mass% Cr to 8 vol.-% at 10 mass% Cr.

Furthermore, the Cr content of the particular phases is increasing with the overall Cr content of the alloy, as shown in Fig. 3. b). The Cr content of the $\text{M}_{23}(\text{C,B})_6$ and iron matrix is showing a proportional dependence on the overall Cr content, whereby values of 35 atom% inside the $\text{M}_{23}(\text{C,B})_6$ and 10 atom% Cr inside the iron phase are reached at 15 mass% overall Cr content. The Cr content of the tetragonal M_2B phase is increasing constantly from 3 up to 12.5 atom% at an overall Cr content of 4.5 mass%. A further increase of the Cr content above 4.5 mass% is stabilizing the orthorhombic M_2B structure with a Cr content of 20 to 42 atom% at 15 mass% overall Cr content. The $\text{M}_3(\text{C,B})$ phase shows only marginal solubility for Cr.

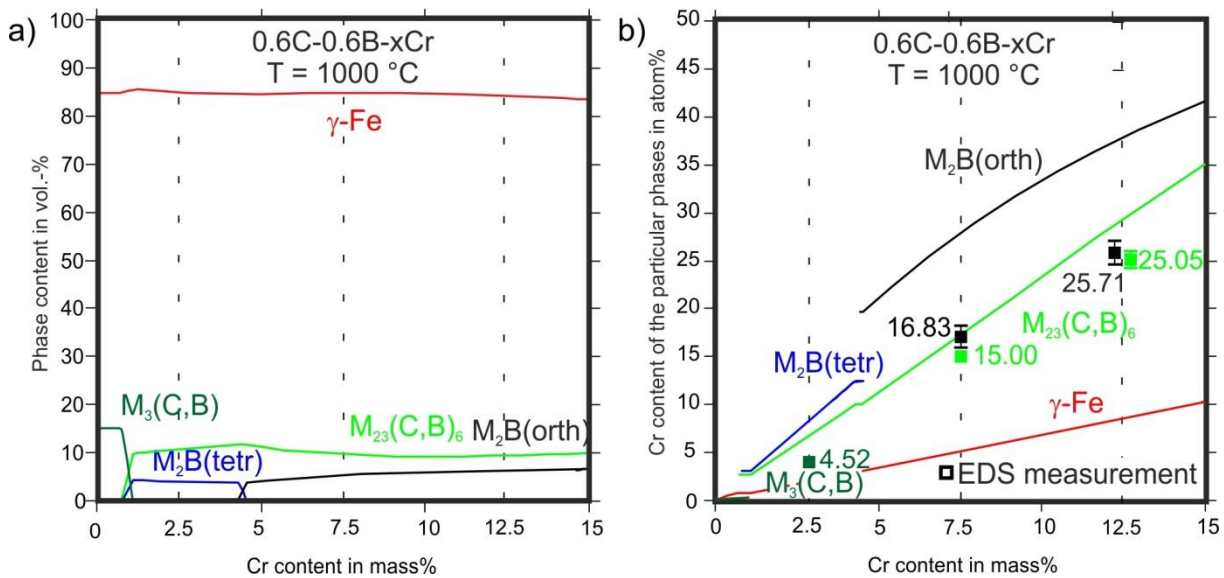


Fig. 3: Thermodynamic calculation of the influence of overall Cr content on a) volume fraction of the phases and b) Cr content of the particular phases for alloy 0.6C-0.6B-xCr at 1000 °C. Experimental EDS measurements at the particular phases are depicted through squares in b)

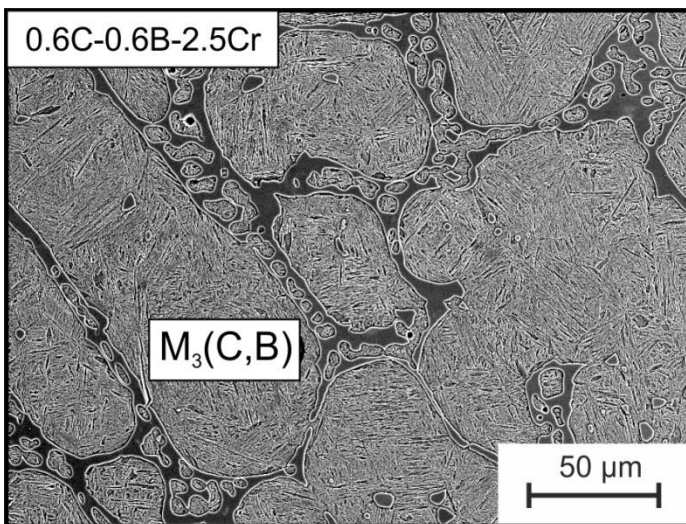


Fig. 4 SEM image of alloy 0.6C-0.6B-2.5Cr in BSE contrast

In contrast to the calculation, the microstructure of alloy 0.6C-0.6B-2.5Cr is showing the coarsened, single-phase eutectic network, which was identified as $M_3(C,B)$ by EBSD point measurement (Fig.4). This is in disagreement with the calculation (see Fig.3), which is indicating the stability of the tetragonal M_2B and $M_{23}(C,B)_6$ phase instead. Differences of calculation and microstructure may be attributed to inaccuracy of the thermodynamically database and also to differences of the technical condition of the alloy and the calculated thermodynamic equilibrium.

Nevertheless, the microstructures of alloy 0.6C-0.6B-7.5Cr (see Fig. 5 a) and 0.6C-0.6B-12.5Cr (Fig. 5 b) are in agreement with the calculations. The eutectic structure is consisting of orthorhombic M_2B and $M_{23}(C,B)_6$ phases. Furthermore, disperse distributed and small precipitates of 1-5 μm in diameter, which appear to be formed in solid state, are present in alloy 0.6C-0.6B-12.5Cr and 0.6C-0.6B-7.5Cr (see Fig. 5 right-side). These precipitates are identified as $M_{23}(C,B)_6$ phase using a EBSD mapping (see Fig.6).

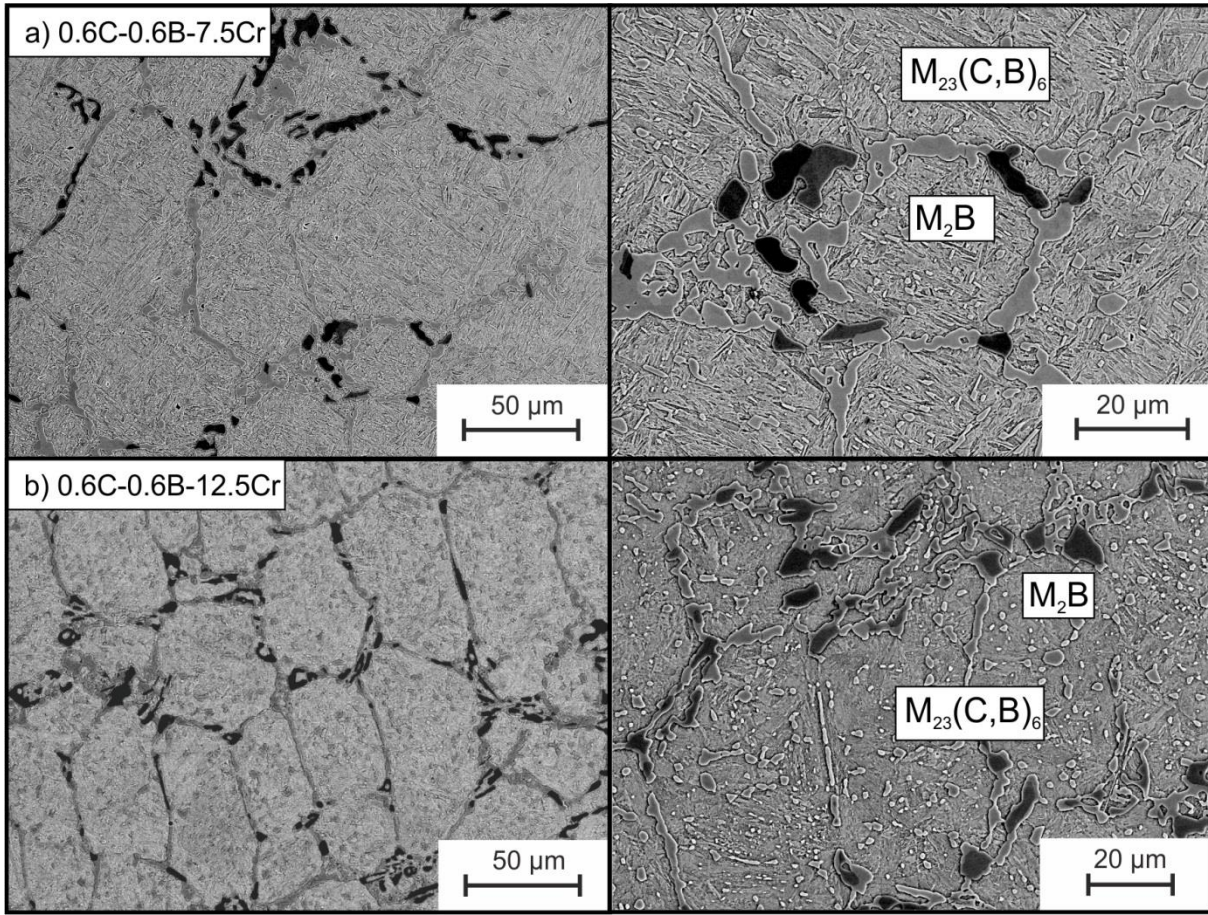


Fig. 5: SEM image of alloy 0.6C-0.6B-7.5Cr and 0.6C-0.6B-12.5Cr in BSE contrast (right: higher magnification)

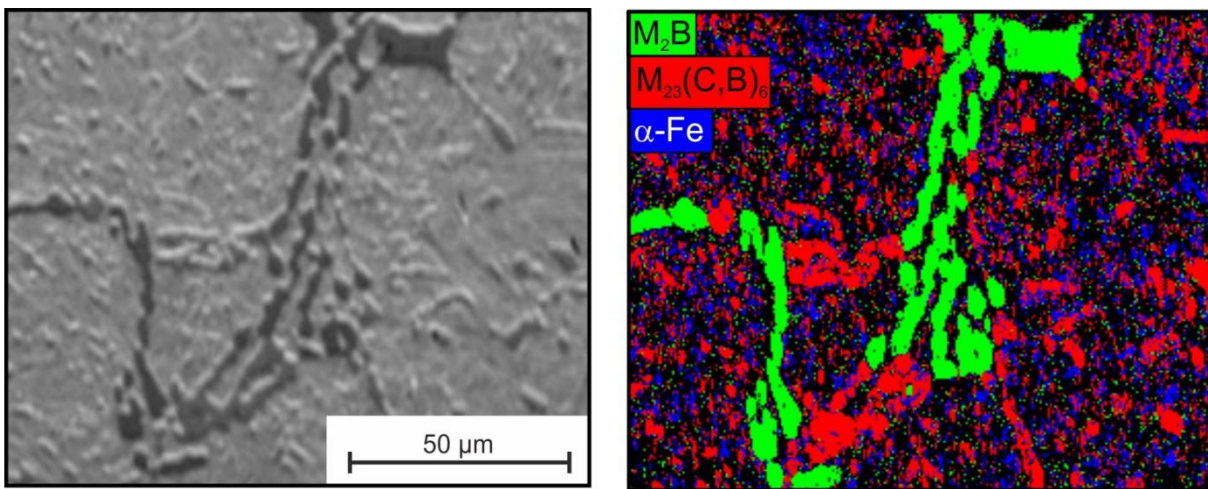


Fig. 6: SEM image in BSE contrast (left) and EBSD-mapping (right) of alloy 0.6C-0.6B-7.5Cr

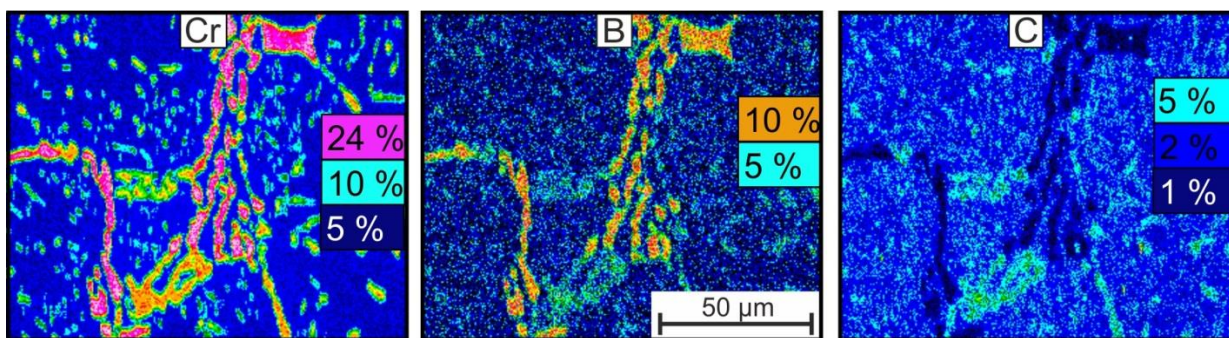


Fig. 7: Quantitative EDS mapping of alloy 0.6C-0.6B-7.5Cr (contents in mass%)

Fig. 7 illustrates the elemental distribution of Cr, B and C in alloy 0.6C-0.6B-7.5Cr for the same area shown in Fig. 6. It is shown that the elements Cr and B are enriched inside the M_2B phase. Though, C is enriched inside the $M_{23}(C,B)_6$ phase, which is also showing an intermediate Cr and B content. In addition, the results of EDS point measurements are depicted in Fig. 3 b). Thereby, it becomes evident that the Cr content present in the M_2B phases is approximately 10 atom% lower than estimated by the calculation. The deviation of the measurement and calculation is smaller in case of the $M_{23}(C,B)_6$ phase, which is overestimated about around 3 atom% by the calculation.

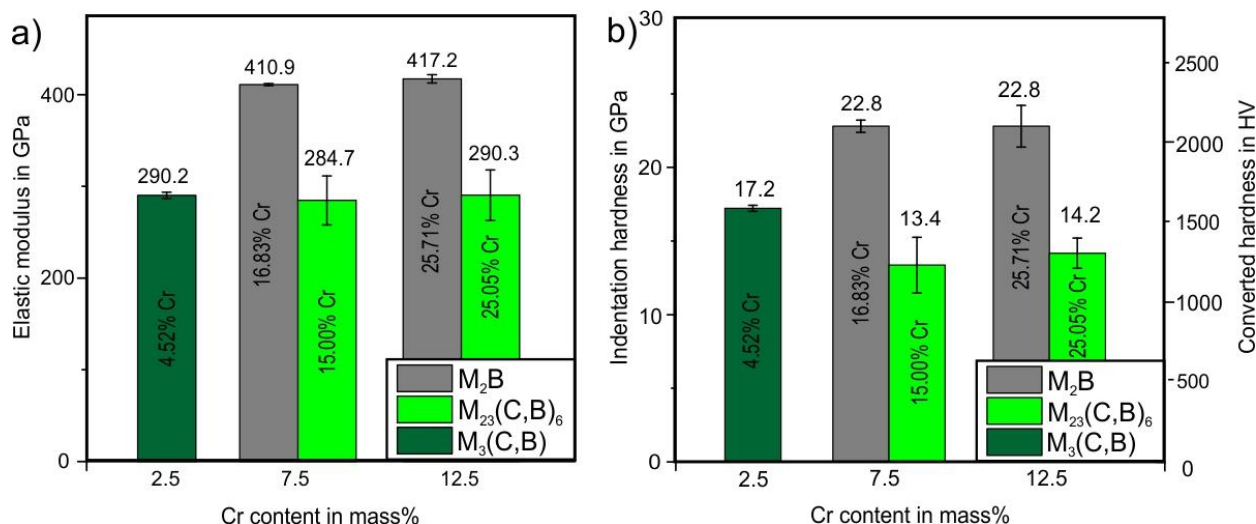


Fig. 8: Elastic modulus and hardness of the particular phases present in alloy 0.6C-0.6B-2.5Cr, 0.6C-0.6B-7.5Cr and 0.6C-0.6B-12.5Cr and EDS results for Cr content of the particular phases in atom%

The elastic modulus of the M_2B , $M_3(C,B)$ and $M_{23}(C,B)_6$ phases is shown in Fig. 8 a). The elastic modulus of $M_3(C,B)$ and $M_{23}(C,B)_6$ phases is almost equal with a value around 290 GPa, while the M_2B phase has a higher modulus with a value between 411 and 417 GPa. Fig 9 b) is showing the indentation hardness of the particular phases. The hardness is increasing from $M_{23}(C,B)_6$ phase with 14 GPa (~1300 HV), to 17.2 GPa (~1600 HV) in case of the $M_3(C,B)$ phase up to 22.8 GPa (2100 HV) for the M_2B phase. A dependency of the elastic modulus or indentation hardness of the M_2B and the $M_{23}(C,B)_6$ phase on Cr contents of the phases is not determined. An investigation of the indentation size effect showed that the indentation hardness of the Fe_2B phase is strongly decreasing up to a depth of 600 nm [15,16]. At higher indentation depth the hardness-curve levels out. However, a constant value is not reached up to an indentation depth of 1200 nm. In this study, the indentation size effect cannot be neglected, because the hardness was evaluated for indentation depths between 600-850 nm. However, the effect is small since an indentation depth of >600 nm is reached. In addition the results are consistent, because the sequence of averaging was kept constant in all measurements. Comparing the hardness of the Cr-rich, orthorhombic M_2B phase with a value for Fe_2B obtained at same indentation depth (~17.5 GPa – 1600 HV) shows, that the Cr-rich, orthorhombic M_2B phase (22.8 GPa - 2100 HV) is considerable harder [16]. This is in accordance with values between 1850-2100 HV0.1 [12,17] and a modulus of 399.4 GPa [5] found in the literature. Thereby it was shown, that the covalent bonds present in the crystal structures were strengthened by the presence of Cr.

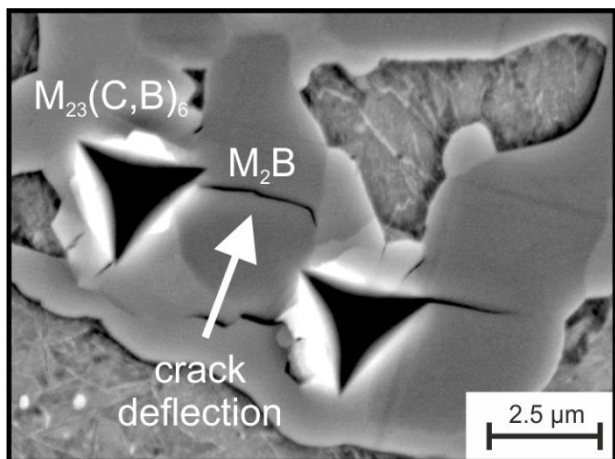


Fig. 9: Crack deflection at the interface M_2B / $M_{23}(C,B)_6$

Moreover, a deflection of cracks at the interfaces of separate hard phase types was observed in case of cracks were induced during the nanoindentation test, as shown in Fig. 9 for the M_2B / $M_{23}(C,B)_6$ interface. In context of wear resistance, a multi-component hard phase structure is beneficial as compared to a single-phased structure to impede crack propagation. This may attribute to the increase of fracture toughness of such hard phase networks.

Concluding, the element Cr is effective to stabilize the M_2B phase with a high hardness of 22.8 GPa, but is also accompanied by the stabilization of the $M_{23}(C,B)_6$ phase, which features a lower hardness (~14 GPa). Thus, further steps of alloy design are aiming on stabilizing the M_2B type boride, instead

of the $M_3(C,B)$, $M_{23}(C,B)_6$ phases and simultaneously maintaining a sufficient C content for martensitic hardening.

In this manner, the effect of the elements Si and Mn is investigated in the following, whereby a C content of 0.75 mass% and a B content of 2 mass% are regarded. The volume content of the particular phases was calculated as a function of the Si content in Fig. 10 a) at a temperature of 700 °C, which corresponds to the stability region of the $M_{23}(C,B)_6$ phase in the pure Fe-C-B system (see Fig. 1 a). It becomes evident that Si is effectively destabilizing the $M_{23}(C,B)_6$ phase and stabilizing $M_3(C,B)$ and M_2B phase. Furthermore, the influence of the alloying element Mn at a temperature of 900 °C and an alloying content of 0.75 mass% C, 2 mass% B and 2.5 mass% Si is shown in Fig. 10 b). It is shown, that the volume content of the M_2B phase is increasing with the Mn content and at the same time the volume content of the $M_3(C,B)$ phase is decreasing.

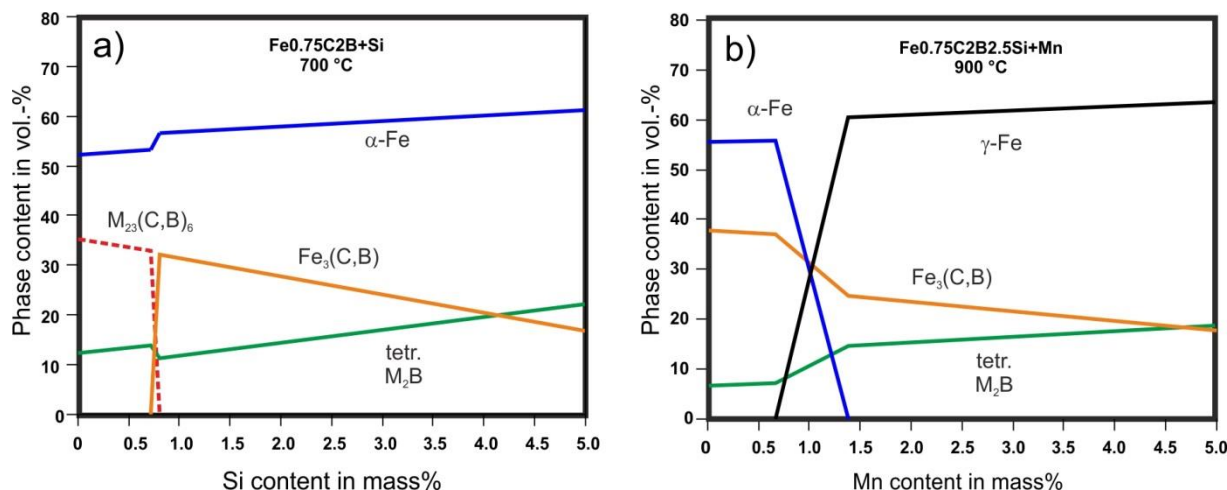


Fig. 10: Phase-quantity graphs of alloy a) Fe_{0.75}C₂B-XSi at 700 °C b) Fe_{0.75}C₂B_{2.5}Si-XMn at 900 °C

In the following, a content of 2.5 mass% Si and 3.8 mass% Mn is used to stabilize ~20 vol.-% M_2B phase and the effect of Cr on the stability of the particular phases in this more technical alloying system is investigated using thermodynamic calculation in Fig. 11 a). In accordance with the effects observed in the quaternary system Fe-C-B-Cr (see Fig. 3), Cr is stabilizing the M_2B and $M_{23}(C,B)_6$ phase in alloy Fe_{0.75}C₂B_{2.5}Si_{3.8}Mn-XCr. However, the volume content of the M_2B phase is increased to 22 vol.-% (for Cr contents >2.2 mass%). Furthermore, the stability range of the tetragonal M_2B phase was extended and the overall Cr content necessary to induce the transformation into the orthorhombic M_2B phase is shifted to 6.8 mass% (instead of 4.5 mass%). A detailed characterization of this alloying system is given in a different study [18]. However, the

most important finding is depicted in Fig. 11 b, whereby hardness and Cr content of the particular phases present in tempered laboratory melts was experimentally measured. It was found that the transformation of the tetragonal into the orthorhombic M_2B phase is occurring at an overall Cr content between 4-6 mass%, which corresponds to a Cr content of 17.5 mass% inside the M_2B phase. The increase of Cr content and transformation of tetragonal into orthorhombic M_2B is accompanied by an increase in hardness of the M_2B phase (17 GPa to 21 GPa). An interdependence of hardness and Cr content was not found in case of the $M_{23}(C,B)_6$ phase.

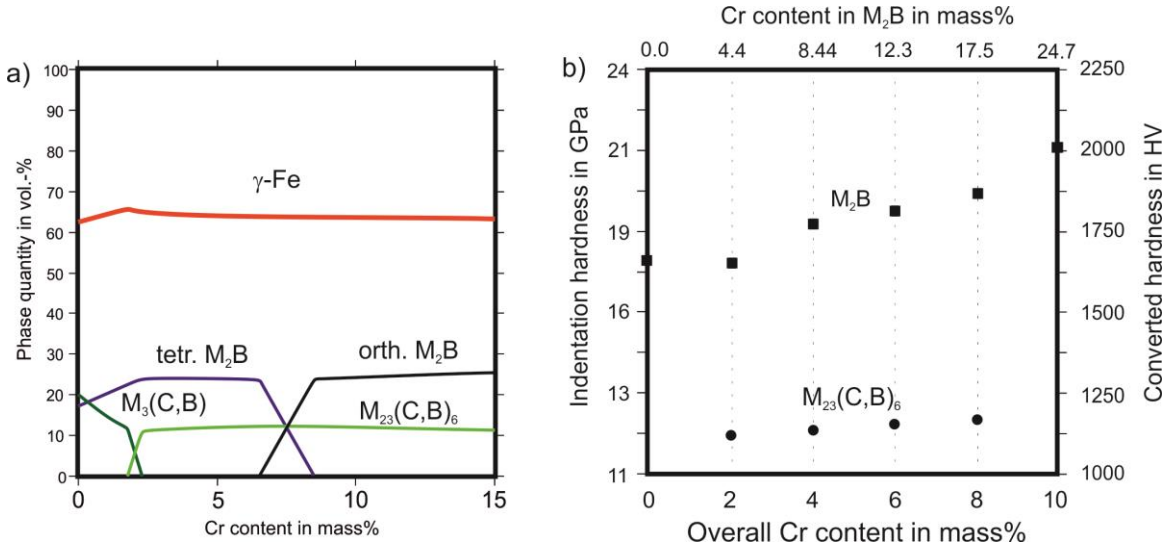


Fig. 11: a) Phase-quantity graph of alloy Fe_{0.75}C₂B_{2.5}Si_{3.8}Mn-XCr at 900 °C b) hardness and of M_2B and $M_{23}(C,B)_6$ phase in dependence of the Cr content [18]

The microstructure of the Fe_{0.75}C₂B_{2.5}Si_{3.8}Mn-XCr with 0 and 10 mass% Cr (see Fig 12) is showing eutectic hard phase structures consisting of the $M_3(C,B)$ and tetragonal M_2B phase (alloy 0Cr) and respectively $M_{23}(C,B)_6$ and orthorhombic M_2B phase (alloy 10Cr) besides a martensitic matrix. Concluding, Cr additions are connected to the stabilization of the Cr-rich orthorhombic M_2B phase but also to the stabilization of $M_{23}(C,B)_6$ phase and destabilization of the $M_3(C,B)$ phase. In addition, a finer distribution of the particular hard phases was achieved inside the microstructure.

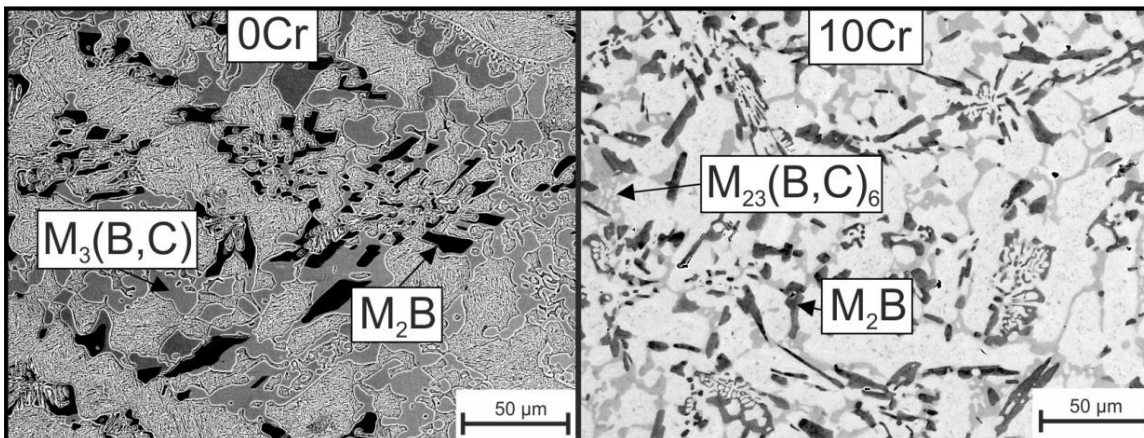


Fig. 12: SEM image in BSE contrast of alloy Fe_{0.75}C₂B_{2.5}Si_{3.8}Mn-XCr with 0 (0Cr-left) and 10 mass% Cr (10Cr-right)

The wear mark of a scratch test, performed for the alloy Fe_{0.75}C₂B_{2.5}Si_{3.8}Mn-10Cr, is shown in Fig 13 a). The governing micro-mechanism is micro-ploughing, in case of the iron matrix. In case of the hard phases pile ups, chips or cracks are not visible, that would indicate the micro mechanisms micro-ploughing, micro-fracturing or micro-cutting. It can be discussed, that the hard phases are plastically deformed and at the same time pushed inside the iron matrix, which is then also plastically deformed. Fig 13 b) is showing the scratch depth of the wear track. A reduction of the scratch depth up to 200 nm is observed, when the scratch passes a hard phase. Thereby, the M_2B

phase is more effective than the $M_{23}(C,B)_6$ phase. This is illustrating the effectiveness of the M_2B type hard phases in wear protection application and also indicating that the M_2B phase is preferable as compared to $M_{23}(C,B)_6$ phase.

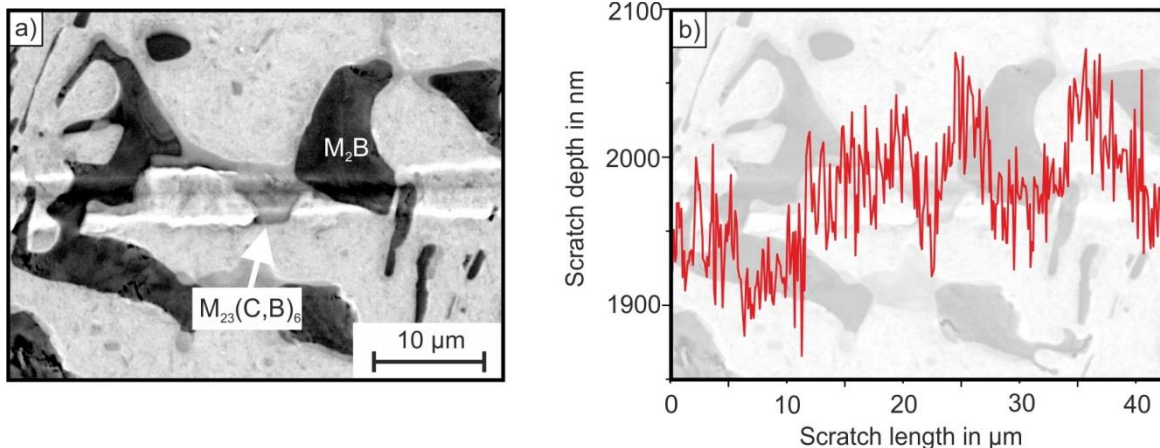


Fig. 13: a) SEM image in BSE contrast of the wear mark of a scratch test for alloy 10Cr (load 100 mN) b) graph of the scratch depth

3. SUMMARY

This contribution is focusing on alloy design based in the Fe-C-B system. The effect of Cr in the quaternary Fe-C-B-Cr was investigated with respect to phase stability and micromechanical properties of particular phases. Furthermore, the elements Cr, Si and Mn were used to stabilize the orthorhombic M_2B phase and to adjust a high Cr content as well as high hardness of the M_2B phase

- The Fe-C-B system was investigated with respect to phase stability and phase properties.
- The M_2B type hard phase was identified as preferable hard phase, because of its high hardness ($\sim 1500\text{-}1700$ HV_{0.01} – 17.5 GPa), low carbon solubility and low metal to metalloid ratio.
- In the Fe-C-B system, the M_2B phase cannot be stabilized by B or C additions without exceeding a hard phase content of 45-50 vol.-%, which is accompanied by a loss of fracture toughness and forming capacity of the alloy.
- It was shown that Cr can be used to stabilize the orthorhombic M_2B phase.
- A hardness of 22.8 GPa (2100 HV) and elastic modulus of 415 GPa was measured for the orthorhombic Cr-rich M_2B phase which corresponds to an increase of $\sim 400\text{-}600$ HV as compared to tetragonal Fe_2B .
- Cr addition is also accompanied by the stabilization of the $M_{23}(C,B)_6$ phase, which features a lower hardness (~ 14 GPa) and lower elastic modulus (~ 290 GPa).
- In the Fe-C-B-Cr system, an interdependency of Cr content of the M_2B and the $M_{23}(C,B)_6$ phases and the micromechanical properties was not determined
- Cr, Si and Mn are used to further stabilize the M_2B phase, whereby a transition of the tetragonal M_2B into the orthorhombic M_2B is occurring at Cr contents between 4 and 6 mass%. This phase transition is connected to an increase of hardness of the M_2B type phases (17 GPa to 21 GPa).

ACKNOWLEDGEMENTS

The authors gratefully acknowledge financial support from the “Deutsche Forschungs Gesellschaft” (DFG) within the project “boron-alloyed tool steels” RO 4523/2-1.

References

- [1] Berns H. Hartlegierungen und Hartverbundwerkstoffe: Gefüge, Eigenschaften, Bearbeitung, Anwendung. Berlin: Springer; 1998.
- [2] Theisen W, Berns H. Ferrous Materials. Berlin, Heidelberg: Springer Berlin Heidelberg; 2008.
- [3] XIE J, SHEN J, CHEN N, Seetharaman S. *Acta Materialia* 2006;54:4653–8.
- [4] Jiang C, Srinivasan SG, Caro A, Maloy SA. *J. Appl. Phys.* 2008;103:043502.
- [5] Xiao B, Feng J, Zhou CT, Xing JD, Xie XJ, Cheng YH, Zhou R. *Physica B: Condensed Matter* 2010;405:1274–8.
- [6] Wang B, Wang DY, Cheng Z, Wang X, Wang YX. *Chemphyschem a European journal of chemical physics and physical chemistry* 2013;14:1245–55.
- [7] DIN Deutsches Institut für Normung e. V. Metallische Werkstoffe - Instrumentierte Eindringprüfung zur Bestimmung der Härte und anderer Werkstoffparameter(14577). Berlin: Beuth Verlag; 2012. [October 23, 2015].
- [8] Lentz J, Röttger A, Theisen W. *Acta Materialia* 2015;99:119–29.
- [9] Berns H, Saltykova A, Röttger A, Heger D. *Steel Res Int.* 2011;82:786–94.
- [10] C. Friedrich, G. Berg, E. Broszeit, C. Berger, Friedrich C, Berg G, Broszeit E, Berger C. *Mat.-wiss. u. Werkstofftech* 1997;28:59–76.
- [11] Lentz J, Röttger A, Theisen W. Gefügeausbildung und mikromechanische Eigenschaften einzelner Phasen von untereutektischen Fe-C-B Legierungen, in: Mayer S, Panzenböck M, Clemens H (Eds.). *Fortschritte in der Metallographie*. Bonn: INVENTUM GmbH; 2014. p. 283–288.
- [12] Ma S, Xing J, Liu G, Yi D, Fu H, Zhang J, Li Y. *Materials Science and Engineering: A* 2010;527:6800–8.
- [13] Feng J, Xiao B, Zhou R, Jiang YH, Cen QH. *Procedia Engineering* 2012;31:676–81.
- [14] Goldfarb I, Kaplan WD, Ariely S, Bamberger M. *Philosophical Magazine A* 1995;72:963–79.
- [15] Campos-Silva I, Hernández-Sánchez E, Rodríguez-Castro G, Rodríguez-Pulido A, López-García C, Ortiz-Domínguez M. *Surface and Coatings Technology* 2011;206:1816–23.
- [16] Rodríguez-Castro G, Campos-Silva I, Chávez-Gutiérrez E, Martínez-Trinidad J, Hernández-Sánchez E, Torres-Hernández A. *Surface and Coatings Technology* 2013;215:291–9.
- [17] Suwattananont N, Petrova R. *Solid State Sciences* 2012;14:1669–72.
- [18] Röttger A, Lentz J, Theisen W. *Materials & Design* 2015;88:420–9.